

Ponderomotive Achromat for Electron Optics: Radially Polarized Annular Focusing and a Round-Lens Corrector Regime

Yuuki Uesugi* and Yuichi Kozawa

*Institute of Multidisciplinary Research for Advanced Materials,
Tohoku University, Katahira 2-1-1, Aoba-ku, Sendai 980-8577, Japan*

(Dated: March 10, 2026)

arXiv:2603.07923v1 [physics.optics] 9 Mar 2026

Abstract

Ponderomotive electron optics has recently attracted attention because structured optical fields can provide round-lens operation with functionalities that are difficult to achieve using conventional electron-optical elements, including negative lens power and negative spherical aberration. A largely unexplored aspect is how ponderomotive lenses disperse with electron energy and whether that dispersion can be engineered for achromatization. Here we show that, for relativistic electrons, longitudinal and transverse optical components exhibit distinct energy dispersion because Lorentz-boost-induced polarization mixing modifies the effective lens action. Focusing a radially polarized annular beam produces two co-located Bessel-like components near focus, a transverse J_1^2 lens and a longitudinal component with relativistic mixing, forming a zero-separation doublet. Using a local Abbe number defined in the energy domain, we derive a single geometry condition for achromatization and evaluate the spot-size performance in a thin-lens model. We also identify parameter regions where the same element yields negative on-axis chromatic aberration, indicating a compact round-lens corrector regime.

Chromatic aberration remains one of the primary constraints in electron optics. When the lens architecture is fixed, an electron-beam energy spread is converted into a focal shift, and that focal shift produces a resolution-degrading disc in the image plane [1–4]. Chromatic aberration correctors exist, but they are often bulky, alignment-sensitive, and strongly coupled to the rest of the column [5, 6]. This motivates the search for compact alternatives, including optical-field approaches in which an electron lens is produced by a ponderomotive interaction with structured light [7–19].

A useful feature of a ponderomotive lens is that its “material” is a light field. The intensity and polarization distribution can be redesigned quickly, and the lens can be reconfigured without changing electrodes or coils. At the same time, if the energy dispersion is effectively fixed, the standard doublet strategy offers limited leverage. In ordinary optics, achromatization is achieved by combining two lenses with different dispersion; in the simplest zero-separation picture, one chooses the lens powers to cancel the first derivative of the total power with respect to wavelength at a design wavelength [20]. If ponderomotive lenses behaved as if they shared essentially the same dispersion, achromatization would force the

* uesugi@tohoku.ac.jp

doublet to zero net power.

The central point of this Letter is that, for relativistic electrons, a longitudinally polarized field does *not* share the same dispersion as a transverse field. A Lorentz-boost effect modifies the effective ponderomotive response of the longitudinal component, producing a dispersion factor that depends on both geometry and energy. This provides a “second material” in the achromat sense, without introducing any additional physical medium. We exploit this with a simple and practical field configuration: focusing a radially polarized annular beam. Near focus, the field naturally decomposes into two Bessel-like components: a transverse component that behaves as a J_1^2 ponderomotive lens and a longitudinal component that behaves as a relativistically mixed Bessel lens, with potentially opposite-sign lens power. Because the components are co-located, the system forms a zero-separation doublet. By choosing the focusing cone angle, we satisfy a first-order achromat condition at a chosen design energy, and we show that the same parameter space includes negative chromatic aberration.

Local Abbe number and achromat condition—We describe achromatization using a local Abbe number defined with respect to electron energy. For a thin lens with focal length $f(\gamma)$ and power $F(\gamma) = 1/f(\gamma)$ written as a function of Lorentz factor γ , we define

$$\nu(\gamma) = \frac{\gamma}{\gamma^2 - 1} \frac{F(\gamma)}{dF/d\gamma}, \quad (1)$$

which plays the role of an Abbe number for an energy-dependent lens power (cf. the wavelength-domain Abbe number in optics; see the Supplemental Material [21]). For a zero-separation lens system, the total power is the sum

$$F_{\text{tot}}(\gamma) = \sum_i F_i(\gamma), \quad (2)$$

and the system is first-order achromatic at $\gamma = \gamma_0$ when $dF_{\text{tot}}/d\gamma$ vanishes at γ_0 . In the present notation, the condition can be written as

$$\sum_i \frac{F_i(\gamma)}{\nu_i(\gamma)} = 0. \quad (3)$$

We now specify the two constituent ponderomotive Bessel lenses. We consider a quasi-Bessel (Bessel-like) optical field whose transverse profile near the axis is well approximated by $J_n^2(Kr)$ [10, 12]. Here $K = k \sin \theta$ is the transverse wavenumber, k is the optical wavenumber,

and θ is the Bessel cone half-angle. We use $\eta \equiv (K/k)^2 = \sin^2 \theta$ as a geometry parameter; in practice, η is set by the focusing optics and the input annulus.

Transverse polarized Bessel lens (\perp)—Taking the common electron and optical beam axis as z , a transversely polarized Bessel field, i.e., polarized perpendicular to z , is effectively restricted to the $n = 1$ case near the optical axis. Its ponderomotive potential is

$$U_{\perp}(r) = \frac{U_0}{\gamma} J_1(Kr)^2, \quad (4)$$

where $U_0 = (h\alpha_{\text{fs}}/(m\omega^2))I_0$ with h Planck's constant, α_{fs} the fine-structure constant, m the electron rest mass, ω the optical angular frequency, and I_0 the peak time-averaged intensity. In the thin-lens toy-model treatment, the transverse J_1^2 lens has power

$$F_{\perp} = F_{J_1} = \frac{\kappa_{J_1}}{\beta^2\gamma^2}, \quad (5)$$

where $\beta = \sqrt{1 - 1/\gamma^2}$ and $\kappa_{J_1} = U_0 K^2 l / (2mc^2)$. Here κ_{J_1} is the signed lens-power coefficient that sets the focusing strength (and its sign) for given (U_0, K, l) , with l an effective interaction length and c the speed of light. The local Abbe number of this transverse Bessel lens is $\nu_{\perp} = -1/2$.

Longitudinal polarized Bessel lens (\parallel) with relativistic mixing—For a longitudinal polarized Bessel field (allowed order $n = 0$), a scalar-field baseline gives a J_0^2 -type potential,

$$U_{\parallel\text{nr}}(r) = \frac{U_0}{\gamma} J_0(Kr)^2. \quad (6)$$

For relativistic electrons, the longitudinal component acquires an additional Lorentz-boost correction relative to the transverse case. Using a phase-based expression for the relativistic correction [22], the ponderomotive potential becomes

$$U_{\parallel} = \frac{U_0}{\gamma} \left[\frac{1}{\gamma^2} J_0^2(Kr) + \eta \left(1 - \frac{1}{\gamma^2} \right) J_1^2(Kr) \right]. \quad (7)$$

This form shows an explicit relativistic mixing between J_0^2 and J_1^2 contributions, with coefficients that depend on γ and η (see the Supplemental Material [21]).

The longitudinal lens power is written as

$$F_{\parallel} = \xi(\gamma; \eta) F_{J_0}, \quad (8)$$

where $F_{J_0} = \kappa_{J_0}/(\beta^2\gamma^2)$ is the J_0^2 -type Bessel-lens power scale with $\kappa_{J_0} = -U_0 K^2 l / (mc^2)$. The dimensionless factor $\xi(\gamma; \eta)$ collects the relativistic mixing weights in Eq.(7) into a single

prefactor multiplying this baseline scale. The resulting correction factor is

$$\xi(\gamma; \eta) = \frac{1}{\gamma^2} - \frac{\eta}{2} \left(1 - \frac{1}{\gamma^2}\right). \quad (9)$$

The dispersion of the longitudinal component is also modified. Its local Abbe number can be written as $\nu_{\parallel} = -\chi/2$, where

$$\chi(\gamma; \eta) = \frac{\eta\gamma^4 - (2 + \eta)\gamma^2}{\eta\gamma^4 - 2(2 + \eta)\gamma^2 + 2 + \eta}. \quad (10)$$

Derivations and plots of $\xi(\gamma; \eta)$ and $\chi(\gamma; \eta)$ are provided in the Supplemental Material [21]. Since χ depends on γ and η , ν_{\parallel} can differ from the fixed $\nu_{\perp} = -1/2$, providing the dispersion contrast required by Eq.(3).

Zero-separation Bessel doublet from a focused radially polarized annular beam—A practical way to generate a Bessel-like focus is to use a narrow annular beam with a strongly focusing lens [23, 24]. If the annular input is radially polarized and focused at a large cone angle, the focal region contains both a transverse (radial) Bessel-like component and a longitudinal (z) component [25–30], as illustrated in Fig.1. Their intensity ratio is set by the focusing geometry as $1 - \sin^2 \theta : \sin^2 \theta$, i.e., $1 - \eta : \eta$. Using the definitions of the primitive Bessel-lens scales above (in particular $\kappa_{J_0} = -2\kappa_{J_1}$, hence $F_{J_0} = -2F_{J_1}$), the two co-located lens powers in the doublet are

$$F_{\perp} = (1 - \eta)F_{J_1}, \quad (11)$$

$$F_{\parallel} = \eta\xi F_{J_0} = -2\eta\xi F_{J_1}. \quad (12)$$

Because the components are spatially overlapped, lens separation is effectively zero, and the achromat condition (3) directly applies.

Using $\nu_{\perp} = -1/2$ and $\nu_{\parallel} = -\chi/2$, the achromat condition at $\gamma = \gamma_0$ becomes

$$\left[\frac{F_{\perp}}{\nu_{\perp}} + \frac{F_{\parallel}}{\nu_{\parallel}} \right]_{\gamma_0} = 2F_{J_1} \left[\left(1 + \frac{2\xi}{\chi}\right) \eta - 1 \right]_{\gamma_0} = 0, \quad (13)$$

which defines the achromat geometry $\eta_{\text{ac}} = \eta_{\text{ac}}(\gamma_0)$ through

$$\eta_{\text{ac}} = \left(1 + 2 \frac{\xi(\gamma_0; \eta_{\text{ac}})}{\chi(\gamma_0; \eta_{\text{ac}})}\right)^{-1}. \quad (14)$$

In practice, η_{ac} is obtained numerically for a chosen design energy.

We denote the total power of the Bessel doublet by

$$F_{\text{Bd}}(\gamma; \eta) = (1 - \eta - 2\eta\xi(\gamma; \eta))F_{J_1}(\gamma), \quad (15)$$

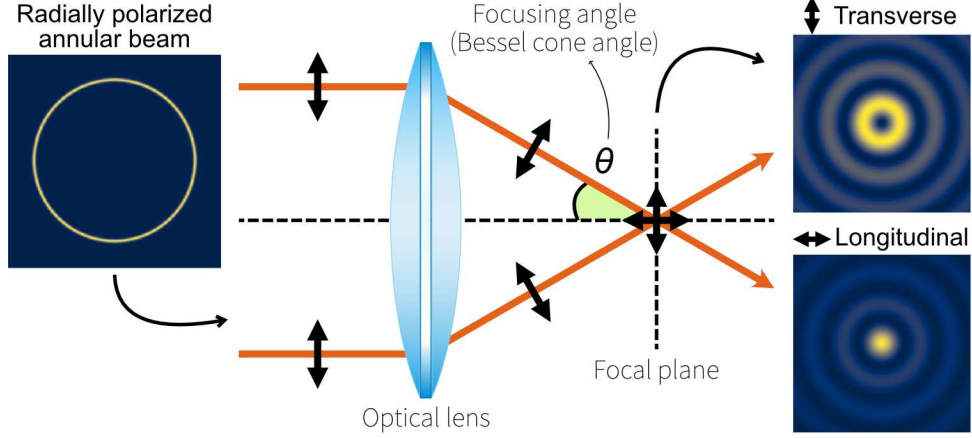


FIG. 1. Conceptual schematic of the zero-separation Bessel doublet formed by focusing a radially polarized annular beam at angle θ . Near the focus, two co-located Bessel-like components appear, with relative weights set by $\eta = \sin^2 \theta$. While the main text discusses the ideal Bessel limit, the profiles shown here are for a finite-width annulus, whose transverse and longitudinal intensities are approximately J_1^2 -like and J_0^2 -like, respectively.

and use it to fix a target focal length at γ_0 . This determines the required field-strength-length product $U_0 l$ (units: eV·m) through the coefficient $\kappa_{J_1} \propto U_0 K^2 l$, at each (γ_0, η) .

Spot-size evaluation—We evaluate the achromatically designed Bessel doublet (aBd) as an objective-lens element in a thin-lens model. Unless noted otherwise, we take $\lambda = 1064$ nm and impose a target focal length of 1 mm at the design energy. A finite energy spread (e.g., $\pm 10\%$ around the design energy) is included, and the transverse spot size is evaluated by separating diffraction, spherical aberration, and chromatic aberration contributions.

Following common electron-optical conventions, the focal shift for a given lens is related to the first-order on-axis chromatic aberration coefficient C_c as $\Delta f = C_c \Delta T / T$, where $T = (\gamma - 1)mc^2$ is the kinetic energy. Using $F = 1/f$ and the local Abbe number definition (1), one can express

$$C_c = -\frac{\gamma}{(\gamma + 1)F\nu}. \quad (16)$$

To connect focal shift to a transverse spot size for a finite energy spread, we define the focal-length change relative to the design energy as

$$\Delta f(\gamma; \gamma_0) = \frac{1}{F_{\text{Bd}}(\gamma; \eta_{\text{ac}})} - \frac{1}{F_{\text{Bd}}(\gamma_0; \eta_{\text{ac}})}, \quad (17)$$

and use $\Delta r(\gamma; \gamma_0) = \alpha \Delta f(\gamma; \gamma_0)$ for the corresponding disc radius at semi-angle α . For an energy spread bounded by γ_{\downarrow} and γ_{\uparrow} , the chromatic contribution is evaluated as

$$\Delta r_c = \max \{ |\Delta r(\gamma_{\downarrow}; \gamma_0)|, |\Delta r(\gamma_{\uparrow}; \gamma_0)| \}. \quad (18)$$

We use the diffraction estimate $\Delta r_d = 0.61 \lambda_e / \alpha$, with λ_e the electron de Broglie wavelength. For spherical aberration, we keep the lowest relevant orders and write

$$\Delta r_s = |C_{s3Bd}(\gamma_0; \eta_{ac})\alpha^3 + C_{s5Bd}(\gamma_0; \eta_{ac})\alpha^5|, \quad (19)$$

where C_{s3Bd} and C_{s5Bd} include the relativistic corrections associated with the longitudinal component; explicit expressions and the term-by-term decomposition used in the zero-separation model are given in the Supplemental Material [21]. Finally, we define

$$\Delta r_{\text{tot}} = \sqrt{\Delta r_d^2 + \Delta r_s^2 + \Delta r_c^2}, \quad (20)$$

and minimize Δr_{tot} over α to obtain an optimal semi-angle α_{opt} .

Figure 2 shows the transverse-aberration (spot-size) characteristics of the aBd and a single transverse J_1^2 Bessel lens for the same target focal length at three representative design energies. In all cases, the aBd gives smaller Δr_c and Δr_s than the singlet. As a result, the optimum semi-angle α_{opt} is larger for the aBd, with the difference most pronounced at lower beam energy. The aBd, however, requires a substantially larger $U_0 l$ than the singlet.

Corrector regime and design maps—Figure 3 summarizes the broader (γ, η) parameter space in terms of the first-order on-axis chromatic-aberration coefficient $C_{cBd}(\gamma; \eta)$ and the required field-strength–length product $U_0 l$ under a focal-length constraint. Here $C_{cBd}(\gamma; \eta) = -\gamma / [(\gamma + 1)F_{Bd}(\gamma; \eta)\nu_{Bd}(\gamma; \eta)]$, i.e., Eq.(16) applied to the composite lens with ν_{Bd} from Eq.(1).

The two panels correspond to different constraints. In the upper panel, $U_0 l$ is fixed and (γ, η) is scanned; the achromat curve $\eta = \eta_{ac}(\gamma)$, equivalently $C_{cBd} = 0$, and the $F_{Bd} = 0$ contour are overlaid. The divergence near $F_{Bd} = 0$ reflects the vanishing net lens power, while regions with $C_{cBd} < 0$ identify corrector-relevant operating points at the chosen strength scale.

In the lower panel, the target focal length is fixed and Eq.(15) is solved for $U_0 l$ at each (γ, η) , yielding the corresponding strength requirement map. Hatched regions indicate $U_0 l < 0$.

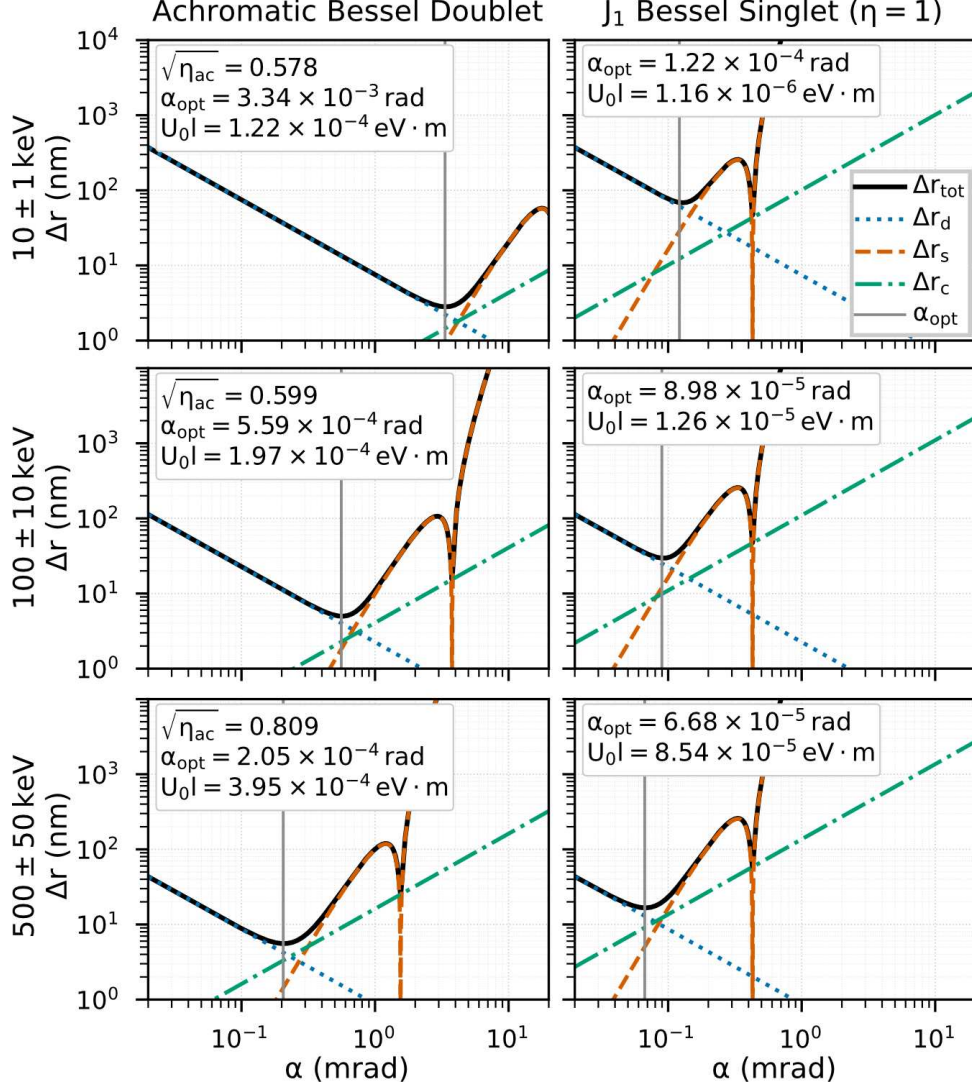


FIG. 2. Transverse-aberration summary comparing an achromatic Bessel doublet (aBd) and a single transverse J_1^2 Bessel lens for the same target focal length of 1 mm at three design energies, with a finite energy spread of $\pm 10\%$. The plotted disc radii are Δr_d , Δr_s , Δr_c , and Δr_{tot} . Additional panels show α_{opt} and the required U_{0l} ; insets for the aBd also show $\sqrt{\eta_{ac}}$.

Discussion and summary—The figures provide a compact picture of where an achromatic ponderomotive round lens is useful and what sets its limits. Figure 2 highlights the main aberration trade-offs. Compared with conventional electromagnetic electron-optical objectives, ponderomotive round lenses tend to carry a relatively large spherical-aberration burden because their effective aperture is limited by the finite transverse extent of the tightly focused optical field; for a transverse J_1 -type Bessel field, for example, the first bright-ring

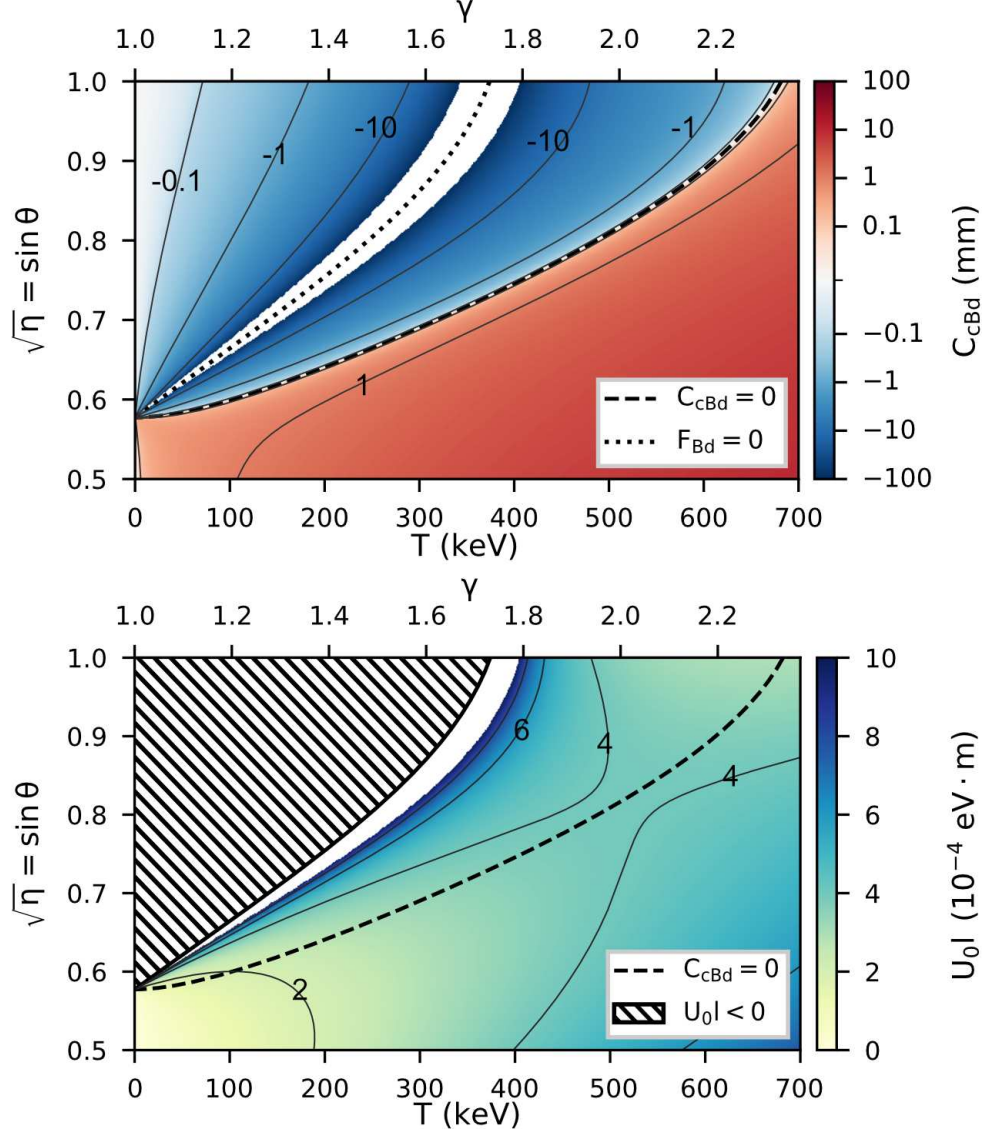


FIG. 3. Design maps: (upper) first-order on-axis chromatic-aberration coefficient $C_{cBd}(\gamma; \eta)$ for fixed $U_0l = 10^{-4}$ eV.m, with the achromat condition $C_{cBd} = 0$ and the $F_{Bd} = 0$ contour overlaid; (lower) required U_0l for a design focal length of 1 mm. Hatched regions in the lower panel indicate $U_0l < 0$. In both panels, white regions indicate values clipped outside the plotted color range.

peak diameter scales as $d_{\text{peak}} \approx 0.59 \lambda / \sqrt{\eta}$, which sets the characteristic transverse lens scale. The aBd mitigates this limitation by canceling the first-order chromatic focal shift at the design energy while also reducing the spherical-aberration contribution through its focusing–defocusing geometry. The resulting increase in α_{opt} therefore reflects a practical gain in usable aperture, albeit at the cost of a larger required U_0l .

With the first-order focal shift canceled at the design energy, the aBd remains effec-

tive even for the large energy spreads used in our illustrative calculations (e.g., $\pm 10\%$ in Fig.2). This tolerance to large energy spread is particularly useful in systems where broad energy modulation or rf-induced energy variation is intrinsic, such as time-lens and ballistic-bunching schemes based on strong longitudinal modulation [31, 32] and rf/linac-based electron optics [33, 34]. The present mechanism is complementary to time-structured chromatic-correction schemes based on space-time-dependent phase modulation of a chirped pulsed electron beam [16]. In our approach, the dispersion contrast originates from the relativistic difference between longitudinal and transverse ponderomotive responses and is implemented within a round-lens geometry.

The main limitation is set by dispersion contrast and efficiency. At low energy, achieving chromatic cancellation while keeping a finite target focal length drives the doublet toward a near-cancellation of the focusing and defocusing components, so that large individual powers are required to leave a small net power. This translates directly into a larger required $U_0 l$ than for a transverse J_1^2 singlet, reaching orders-of-magnitude differences in the 10 keV example of Fig.2. The broader maps in Fig.3 show that this trade-off persists around the achromat locus $\eta_{ac}(\gamma)$: moderate negative C_{cBd} remains reachable at manageable strength cost, whereas pushing toward stronger correction near $F_{Bd} = 0$ rapidly becomes expensive.

Relaxing the constraints of the present single-beam, zero-separation realization is an obvious direction. Independent control of the transverse and longitudinal weights (or their field scales) and/or a finite separation should broaden the feasible region and reduce the near-cancellation penalty at a given target focal length, although low-energy operation will still tend to be excitation-demanding when strong dispersion compensation is required. A natural extension is therefore a hybrid layout in which an electrostatic focusing element supplies additional dispersion contrast while an optical-field element provides round defocusing without resorting to multipole corrector geometries.

In summary, relativistic longitudinal polarization mixing creates the dispersion contrast required for a zero-separation achromat in ponderomotive electron optics. A focused radially polarized annular beam naturally forms a co-located Bessel doublet whose geometry can be chosen to satisfy a first-order achromat condition at a selected design energy. The same framework also yields a round-lens corrector regime with $C_{cBd} < 0$.

Acknowledgments—We thank T. Sannomiya and G. Matsuoka for discussions on this work. This work was supported in part by JSPS KAKENHI Grant No. JP25K22000,

JST FOREST Grant Nos. JPMJFR222F and JPMJFR223E, AMED under Grant No. JP24wm0625105, and NEDO (New Energy and Industrial Technology Development Organization) under Project No. JPNP14004.

SUPPLEMENTAL MATERIAL

Notation and conventions

Throughout this Supplemental Material, we use the thin-lens power $F = 1/f$, where f is the focal length. The electron Lorentz factor is γ , $\beta = \sqrt{1 - 1/\gamma^2}$, and the electron speed is $v = \beta c$, with c the speed of light and m the electron rest mass. The electron de Broglie wavelength is $\lambda = h/(\beta\gamma mc)$. Optical quantities are the angular frequency ω and wavenumber k . For a Bessel cone, the transverse wavenumber is $K = k \sin \theta$ with cone half-angle θ , and we define $\eta = (K/k)^2 = \sin^2 \theta$. The ponderomotive energy scale is

$$U_0 = \frac{h \alpha_{\text{fs}}}{m\omega^2} I_0, \quad (\text{S1})$$

where h is Planck's constant, α_{fs} is the fine-structure constant, and I_0 is a time-averaged intensity scale used to normalize the field profile. An effective interaction length is denoted by l . Analytic expressions for Bessel-lens power and low-order spherical coefficients follow the thin-lens Bessel-lens model summarized in Ref. [12].

S1. ENERGY-DOMAIN LOCAL ABBE NUMBER AND THE FIRST-ORDER ACHROMAT CONDITION

We introduce a local Abbe-number measure for an energy-dependent lens power and derive the first-order achromat condition for a zero-separation system. In optics, dispersion is commonly summarized by the Abbe number defined from discrete refractive indices at standard wavelengths [20]. Here we introduce a local counterpart that measures how rapidly a thin-lens power varies with wavelength.

For a thin lens with wavelength-independent shape factor S (set by curvature and thickness in the paraxial limit), the power can be written as $F(\lambda) = S[n(\lambda) - 1]$, and hence

$dF/d\lambda = S dn/d\lambda$. We define the local Abbe number in the wavelength domain by

$$\nu(\lambda) = -\frac{F(\lambda)}{\lambda (dF/d\lambda)}. \quad (\text{S2})$$

This definition is used here as a compact local measure of the wavelength dispersion of $F(\lambda)$.

For a composite system with total power F_{tot} , expand around a design wavelength λ_0 :

$$F_{\text{tot}}(\lambda) = F_{\text{tot}}(\lambda_0) + (\lambda - \lambda_0) \left. \frac{dF_{\text{tot}}}{d\lambda} \right|_{\lambda_0} + \frac{1}{2}(\lambda - \lambda_0)^2 \left. \frac{d^2F_{\text{tot}}}{d\lambda^2} \right|_{\lambda_0} + \dots \quad (\text{S3})$$

For a zero-separation (co-located) system,

$$F_{\text{tot}}(\lambda) = \sum_i F_i(\lambda). \quad (\text{S4})$$

First-order achromatization at λ_0 requires the linear term in Eq. (S3) to vanish:

$$\left. \frac{dF_{\text{tot}}}{d\lambda} \right|_{\lambda_0} = \sum_i \left. \frac{dF_i}{d\lambda} \right|_{\lambda_0} = 0. \quad (\text{S5})$$

Using Eq. (S2), i.e. $dF/d\lambda = -(1/\lambda) F/\nu$, Eq. (S5) becomes

$$\sum_i \frac{F_i(\lambda_0)}{\nu_i(\lambda_0)} = 0. \quad (\text{S6})$$

If one additionally enforces $d^2F_{\text{tot}}/d\lambda^2|_{\lambda_0} = 0$, the quadratic term in Eq. (S3) is also canceled, corresponding to the usual apochromat condition.

We now rewrite the local Abbe number in the energy domain by changing the independent variable from λ to γ . Since $\lambda = h/(\beta\gamma mc) \propto (\gamma^2 - 1)^{-1/2}$, we have

$$\frac{d\lambda}{d\gamma} = -\lambda \frac{\gamma}{\gamma^2 - 1}. \quad (\text{S7})$$

Using $dF/d\lambda = (dF/d\gamma)(d\gamma/d\lambda)$ in Eq. (S2), we define the energy-domain local Abbe number as

$$\nu(\gamma) = \frac{\gamma}{\gamma^2 - 1} \frac{F(\gamma)}{dF/d\gamma}. \quad (\text{S8})$$

Equivalently,

$$\frac{dF}{d\gamma} = \frac{\gamma}{\gamma^2 - 1} \frac{F(\gamma)}{\nu(\gamma)}. \quad (\text{S9})$$

Therefore, for a zero-separation system, first-order achromatization at a design point γ_0 requires

$$\left. \frac{dF_{\text{tot}}}{d\gamma} \right|_{\gamma_0} = \sum_i \left. \frac{dF_i}{d\gamma} \right|_{\gamma_0} = 0 \iff \sum_i \frac{F_i(\gamma_0)}{\nu_i(\gamma_0)} = 0, \quad (\text{S10})$$

which is the first-order achromat condition used in the main text.

S2. RELATIVISTIC LONGITUDINAL PONDEROMOTIVE POTENTIAL AND BESSEL MIXING

We outline the main steps leading to the longitudinal ponderomotive potential used in the main text, based on the phase formulation of Axelrod *et al.* [22]. We denote by e the elementary charge, by \hbar the reduced Planck constant, and by \mathbf{n}_z the unit vector along the electron propagation axis z .

Axelrod *et al.* express the second-order phase shift of a relativistic electron interacting with an electromagnetic field as

$$\Delta\Phi = -\frac{1}{\hbar} \int dt \frac{e^2}{2\gamma m} [(\mathbf{A} - \nabla G)^2 - \beta^2 (A_z - \partial_z G)^2], \quad (\text{S11})$$

where $\mathbf{A} = (A_r, A_\phi, A_z)$ is the vector potential and the gauge function G is defined by

$$G(\mathbf{r}, t) = c\beta \int_{-\infty}^t dt' A_z(\mathbf{r} - (t - t')c\beta \mathbf{n}_z, t'). \quad (\text{S12})$$

We consider an ideal monochromatic Bessel field and take the vector potential to be purely longitudinal:

$$A_x = A_y = 0, \quad A_z(r, t) = A_0 J_0(Kr) \cos(\omega t), \quad (\text{S13})$$

with amplitude A_0 and transverse wavenumber $K = k \sin \theta$. Substituting Eq. (S13) into Eq. (S12), the radial derivative $\partial_r G$ is proportional to $\partial_r J_0(Kr) = -K J_1(Kr)$, so the $(\mathbf{A} - \nabla G)^2$ term in Eq. (S11) generates a contribution proportional to $J_1^2(Kr)$, with a geometry prefactor set by $\eta = (K/k)^2$. The A_z^2 term contributes $J_0^2(Kr)$ with a different γ -dependent weight through the longitudinal subtraction term. Carrying out the cycle average over the optical period and writing the averaged phase shift as $\Delta\bar{\Phi} = -(1/\hbar)U_{\parallel}$, one obtains

$$U_{\parallel}(r) = \frac{U_0}{\gamma} \left[\frac{1}{\gamma^2} J_0^2(Kr) + \eta \left(1 - \frac{1}{\gamma^2} \right) J_1^2(Kr) \right], \quad (\text{S14})$$

which is the longitudinal potential used in the main text.

S3. POWER AND DISPERSION OF THE TRANSVERSE AND LONGITUDINAL BESSEL COMPONENTS

This section summarizes the thin-lens Bessel-lens parametrization used for the transverse and longitudinal components and highlights the characteristic features of the longitudinal

correction factors $\xi(\gamma; \eta)$ and $\chi(\gamma; \eta)$. Analytic expressions for the Bessel-lens power scales and spherical terms follow Ref. [12].

S3.A. Power scales and the factor $\xi(\gamma; \eta)$

For the transverse J_1^2 component, the lens power is written as

$$F_{J_1}(\gamma) = \frac{\kappa_{J_1}}{\beta^2 \gamma^2}, \quad \kappa_{J_1} = \frac{U_0 K^2 l}{2mc^2}. \quad (\text{S15})$$

For the longitudinal component, we introduce a scalar-field baseline J_0^2 power scale

$$F_{J_0}(\gamma) = \frac{\kappa_{J_0}}{\beta^2 \gamma^2}, \quad \kappa_{J_0} = -\frac{U_0 K^2 l}{mc^2}. \quad (\text{S16})$$

and use it as a reference for the relativistically mixed longitudinal response derived in Sec. S2.

From Eq. (S14), the longitudinal power can be written as

$$F_{\parallel}(\gamma; \eta) = \frac{1}{\gamma^2} F_{J_0}(\gamma) + \eta \left(1 - \frac{1}{\gamma^2} \right) F_{J_1}(\gamma). \quad (\text{S17})$$

Within the present parametrization, the primitive scales share the same (U_0, K, l) dependence, so $\kappa_{J_0} = -2\kappa_{J_1}$ and hence $F_{J_0} = -2F_{J_1}$. Using $F_{J_1} = -(1/2)F_{J_0}$ in Eq. (S17) gives

$$F_{\parallel}(\gamma; \eta) = \xi(\gamma; \eta) F_{J_0}(\gamma), \quad (\text{S18})$$

where

$$\xi(\gamma; \eta) = \frac{1}{\gamma^2} - \frac{\eta}{2} \left(1 - \frac{1}{\gamma^2} \right). \quad (\text{S19})$$

The factor ξ sets both the magnitude and the sign of the longitudinal power relative to the baseline scale F_{J_0} . Figure S1 (left) plots $\xi(\gamma; \eta)$ for $\eta = 1, 1/2$ and $1/3$. It satisfies $\xi(1; \eta) = 1$ and $\xi(\gamma \rightarrow \infty; \eta) \rightarrow -\eta/2$. Its zero-crossing occurs at

$$\xi(\gamma_c; \eta) = 0 \quad \Rightarrow \quad \gamma_c(\eta) = \sqrt{1 + \frac{2}{\eta}}, \quad (\text{S20})$$

so the longitudinal component changes sign at $\gamma = \gamma_c$.

S3.B. Dispersion factor $\chi(\gamma; \eta)$ and its singular structure

The transverse component has the fixed dispersion

$$\nu_{\perp} = -\frac{1}{2}, \quad (\text{S21})$$

obtained by substituting Eq. (S15) into the energy-domain definition $\nu(\gamma) = \gamma(\gamma^2 - 1)^{-1}F/(dF/d\gamma)$ (Sec. S1). For the longitudinal component, applying the same definition to $F_{\parallel}(\gamma; \eta)$ yields

$$\nu_{\parallel}(\gamma; \eta) = -\frac{1}{2}\chi(\gamma; \eta), \quad (\text{S22})$$

with

$$\chi(\gamma; \eta) = \frac{\eta\gamma^4 - (2 + \eta)\gamma^2}{\eta\gamma^4 - 2(2 + \eta)\gamma^2 + (2 + \eta)}. \quad (\text{S23})$$

Figure S1 (right) plots $\chi(\gamma; \eta)$ for $\eta = 1, 1/2$ and $1/3$. The function χ satisfies $\chi(1; \eta) = 1$ and $\chi(\gamma \rightarrow \infty; \eta) \rightarrow 1$. Its numerator contains the same factor $(\eta\gamma^2 - (2 + \eta))$ as ξ , so χ crosses zero at the same $\gamma_c(\eta)$ given by Eq. (S20). In addition, χ has a pole where the denominator vanishes, which corresponds to $dF_{\parallel}/d\gamma = 0$ and therefore to a divergence of the local Abbe number $\nu_{\parallel} \propto F_{\parallel}/(dF_{\parallel}/d\gamma)$. Writing $x = \gamma^2$, the denominator is a quadratic in x and has two roots; the physically relevant pole lies at $x > 1$:

$$\gamma_d(\eta) = \sqrt{\frac{(2 + \eta) + \sqrt{2(2 + \eta)}}{\eta}}. \quad (\text{S24})$$

For $\gamma > 1$, χ crosses zero at $\gamma = \gamma_c$ and diverges at $\gamma = \gamma_d$, before approaching $\chi \rightarrow 1$ at higher γ .

S4. THIRD-ORDER SPHERICAL ABERRATION IN THE ZERO-SEPARATION DOUBLET

This section summarizes the third-order spherical-aberration coefficient used in the spot-size model and presents compact expressions for the co-located Bessel doublet in terms of the primitive J_1^2 and J_0^2 baselines. Following Ref. [12], a denotes the object-to-aperture distance in the Bessel-lens geometry (often $a \simeq f$ in an objective-lens-like configuration).

For the transverse J_1^2 baseline lens,

$$C_{s3J_1}(\gamma) = -\frac{K^2 a^4}{2} F_{J_1}(\gamma), \quad (\text{S25})$$

and for the scalar-field longitudinal baseline J_0^2 lens,

$$C_{s3J_0}(\gamma) = -\frac{3K^2 a^4}{8} F_{J_0}(\gamma). \quad (\text{S26})$$

Within the present Bessel-lens parametrization, the primitives share the same (U_0, K, l) dependence so that $F_{J_0} = -2F_{J_1}$, implying $C_{s3J_0} = -(3/2)C_{s3J_1}$.

For the relativistically mixed longitudinal component, the mixing weights that generate the power also generate the third-order spherical coefficient:

$$C_{s3\parallel}(\gamma; \eta) = \frac{1}{\gamma^2} C_{s3J_0}(\gamma) + \eta \left(1 - \frac{1}{\gamma^2}\right) C_{s3J_1}(\gamma). \quad (\text{S27})$$

Using $C_{s3J_1} = -(2/3)C_{s3J_0}$, Eq. (S27) can be written in the compact J_0 -based form

$$C_{s3\parallel}(\gamma; \eta) = \xi_{s3}(\gamma; \eta) C_{s3J_0}(\gamma), \quad (\text{S28})$$

with

$$\xi_{s3}(\gamma; \eta) = \frac{1}{\gamma^2} - \frac{2\eta}{3} \left(1 - \frac{1}{\gamma^2}\right). \quad (\text{S29})$$

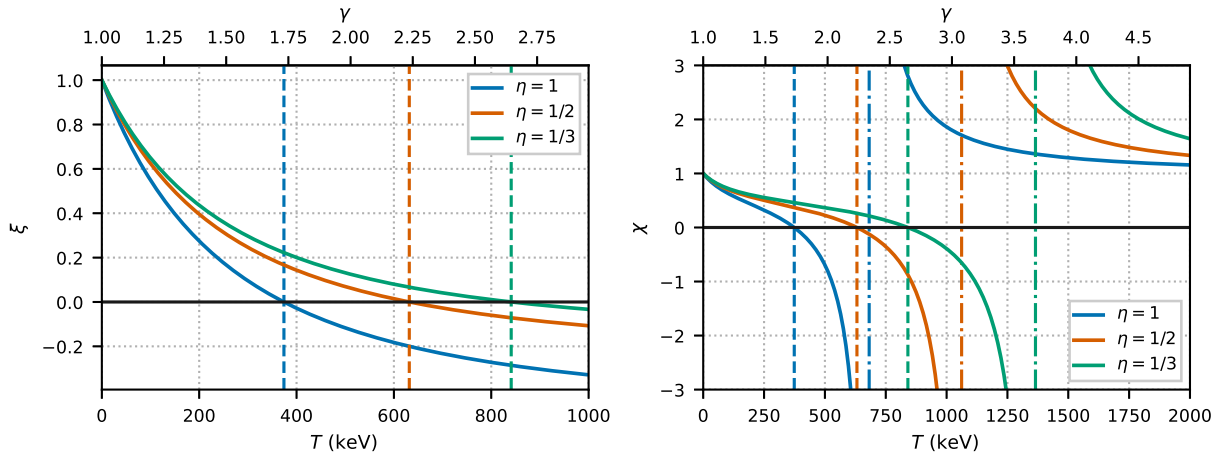


FIG. S1. Representative longitudinal correction factors: (left) $\xi(\gamma; \eta)$ and (right) $\chi(\gamma; \eta)$ as functions of γ for $\eta = 1, 1/2$, and $1/3$. Vertical lines mark the zero crossing at $\gamma_c(\eta)$ (dashed) and the pole at $\gamma_d(\eta)$ (dash-dotted).

For the co-located doublet formed by weights $(1 - \eta)$ and η , we define

$$C_{s3Bd}(\gamma; \eta) = (1 - \eta) C_{s3J_1}(\gamma) + \eta C_{s3\parallel}(\gamma; \eta). \quad (\text{S30})$$

Substituting Eq. (S28) and using $C_{s3J_0} = -(3/2) C_{s3J_1}$ yields a compact J_1 -based form,

$$C_{s3Bd}(\gamma; \eta) = \zeta_{s3}(\gamma; \eta) C_{s3J_1}(\gamma), \quad (\text{S31})$$

where

$$\zeta_{s3}(\gamma; \eta) = (1 - \eta) - \frac{3\eta}{2} \xi_{s3}(\gamma; \eta) = (1 - \eta) - \frac{3\eta}{2\gamma^2} + \eta^2 \left(1 - \frac{1}{\gamma^2}\right). \quad (\text{S32})$$

This J_1 -based expression is convenient when comparing with the doublet power written in terms of F_{J_1} in the main text.

The corresponding fifth-order coefficients (C_{s5J_1} , C_{s5J_0} , $C_{s5\parallel}$, and C_{s5Bd}) follow by the same procedure using the C_{s5} .

-
- [1] O. Scherzer, “Über einige Fehler von Elektronenlinsen,” *Z. Phys.* **101**, 593 (1936).
 - [2] P. W. Hawkes and E. Kasper, *Principles of Electron Optics* (Academic Press, London, 1989).
 - [3] H. Rose, “Aberration correction in electron microscopy,” *J. Electron Microsc.* **58**, 77 (2009).
 - [4] P. W. Hawkes, “The correction of electron lens aberrations,” *Ultramicroscopy* **156**, A1 (2015).
 - [5] M. Haider, P. Hartel, H. Müller, S. Uhlemann, and J. Zach, “Current and future aberration correctors for the improvement of resolution in electron microscopy,” *Philos. Trans. R. Soc. A* **367**, 3665–3682 (2009).
 - [6] M. Linck *et al.*, “Chromatic Aberration Correction for Atomic Resolution TEM Imaging from 20 to 80 kV,” *Phys. Rev. Lett.* **117**, 076101 (2016).
 - [7] V. G. Minogin, “Electron beam deflection, focusing, and collimation by a femtosecond laser lens,” *Quantum Electron.* **39**, 1095–1098 (2009).
 - [8] F. J. García de Abajo and A. Konečná, “Optical Modulation of Electron Beams in Free Space,” *Phys. Rev. Lett.* **126**, 123901 (2021).
 - [9] Y. Uesugi, Y. Kozawa, and S. Sato, “Electron round lenses with negative spherical aberration by a tightly focused cylindrically polarized light beam,” *Phys. Rev. Applied* **16**, L011002 (2021).

- [10] Y. Uesugi, Y. Kozawa, and S. Sato, “Properties of electron lenses produced by ponderomotive potential with Bessel and Laguerre-Gaussian beams,” *J. Opt.* **24**, 054013 (2022).
- [11] M. C. C. Mihaila, P. Weber, M. Schneller, L. Grandits, S. Nimmrichter, and T. Juffmann, “Transverse Electron-Beam Shaping with Light,” *Phys. Rev. X* **12**, 031043 (2022).
- [12] Y. Uesugi, “The properties of ponderomotive lenses,” *Adv. Imaging Electron Phys.* **228**, 1–41 (2023).
- [13] M. C. C. Mihaila and M. Kozák, “Design for light-based spherical aberration correction of ultrafast electron microscopes,” *Opt. Express* **33**, 758–775 (2025).
- [14] J. Ribbing, G. Perosa, and V. Goryashko, “Relativistic ponderomotive force in the regime of extreme focusing,” *Opt. Lett.* **50**, 2093–2096 (2025).
- [15] Y. Uesugi and Y. Kozawa, “Crossed ponderomotive lenses for spherical aberration correction in electron optics,” *Phys. Rev. A* **112**, 013507 (2025).
- [16] M. C. C. Mihaila, N. Laštovičková Streshkova, and M. Kozák, “Light-Based Chromatic Aberration Correction of Ultrafast Electron Microscopes,” *Phys. Rev. Lett.* **134**, 203802 (2025).
- [17] M. C. C. Mihaila, P. Koutenský, K. Moriová, and M. Kozák, “Light-based electron aberration corrector,” *Nat. Photonics* **19**, 1309–1314 (2025).
- [18] Z. Nekula, T. Juffmann, and A. Konečná, “Laser-based aberration corrector,” arXiv:2501.16501 (2025).
- [19] V. Rollo, F. Kato, H. Taira, R. Nagao, G. Privault, S. Weber, M. Hada, and A. Arbouet, “Ponderomotive electron–light interactions in multi-electron pulses,” *New J. Phys.* **28**, 024101 (2026).
- [20] M. Born and E. Wolf, *Principles of Optics* (Cambridge University Press, Cambridge, 1999).
- [21] See the “Supplemental Material” section.
- [22] J. J. Axelrod, S. L. Campbell, O. Schwartz, C. Turnbaugh, R. M. Glaeser, and H. Müller, “Observation of the Relativistic Reversal of the Ponderomotive Potential,” *Phys. Rev. Lett.* **124**, 174801 (2020).
- [23] J. Durnin, “Diffraction-Free Beams,” *Phys. Rev. Lett.* **58**, 1499 (1987).
- [24] R. M. Herman and T. A. Wiggins, “Production and uses of diffractionless beams,” *J. Opt. Soc. Am. A* **8**(6), 932–942 (1991).
- [25] B. Richards and E. Wolf, “Electromagnetic diffraction in optical systems, II. Structure of the image field in an aplanatic system,” *Proc. R. Soc. Lond. A* **253**(1274), 358–379 (1959).

- [26] S. Quabis, R. Dorn, M. Eberler, O. Glöckl, and G. Leuchs, “Focusing light to a tighter spot,” *Opt. Commun.* **179**(1–6), 1–7 (2000).
- [27] K. S. Youngworth and T. G. Brown, “Focusing of high numerical aperture cylindrical-vector beams,” *Opt. Express* **7**(2), 77–87 (2000).
- [28] R. Dorn, S. Quabis, and G. Leuchs, “Sharper Focus for a Radially Polarized Light Beam,” *Phys. Rev. Lett.* **91**, 233901 (2003).
- [29] C. J. R. Sheppard and A. Choudhury, “Annular pupils, radial polarization, and superresolution,” *Appl. Opt.* **43**(22), 4322–4327 (2004).
- [30] Y. Kozawa and S. Sato, “Focusing property of a double-ring-shaped radially polarized beam,” *Opt. Lett.* **31**(6), 820–822 (2006).
- [31] S. A. Hilbert, C. Uiterwaal, B. Barwick, H. Batelaan, and A. H. Zewail, “Temporal lenses for attosecond and femtosecond electron pulses,” *Proc. Natl. Acad. Sci. U.S.A.* **106**(26), 10558–10563 (2009).
- [32] M. Kozák, N. Schönenberger, and P. Hommelhoff, “Ponderomotive Generation and Detection of Attosecond Free-Electron Pulse Trains,” *Phys. Rev. Lett.* **120**, 103203 (2018).
- [33] W. Verhoeven, J. F. M. van Rens, E. R. Kieft, P. H. A. Mutsaers, and O. J. Luiten, “High quality ultrafast transmission electron microscopy using resonant microwave cavities,” *Ultramicroscopy* **188**, 85–89 (2018).
- [34] T. Sannomiya, Y. Arai, K. Nagayama, and Y. Nagatani, “Transmission Electron Microscope Using a Linear Accelerator,” *Phys. Rev. Lett.* **123**, 150801 (2019).